

Real-Time Long Horizon Air Quality Forecasting via Group-Relative Policy Optimization

Inha Kang¹, Eunki Kim¹, Wonjeong Ryu¹, Jaeyo Shin¹, Seungjun Yu¹
Yoon-Hee Kang², Seongeun Jeong², Eunhye Kim³, Soontae Kim², Hyunjung Shim¹

¹KAIST AI ²Ajou University ³Kunsan University

{rkswlsj13, eunkikim, petac, jaeyo-shin, seungjunyu, kateshim}@kaist.ac.kr

{ykang, atmos1214, soontaekim}@ajou.ac.kr ekim@kunsan.ac.kr

Abstract

Accurate long horizon forecasting of particulate matter (PM) concentration fields is essential for operational public health decisions. However, achieving reliable forecasts remains challenging in regions with complex terrain and strong atmospheric dynamics such as East Asia. While foundation models such as Aurora offer global generality, they often miss region-specific dynamics and rely on non-real-time inputs, limiting their practical utility for localized warning systems. To address this gap, we construct and release the real-world observations and high-resolution CMAQ-OBS dataset for East Asia, reducing regional error by 59.5% and enabling real-time 48–120 hour forecasts critical for public health alerts. However, standard point-wise objectives cannot reflect asymmetric operational costs, where false alarms deteriorate public trust while missed severe events endanger populations. This cost mismatch causes SFT models to over-predict and yield high False Alarm Rates. We introduce Group-Relative Policy Optimization (GRPO) with class-wise rewards and curriculum rollout to align predictions with operational priorities. Experimental results demonstrate that our framework significantly improves the reliability of the forecast. Compared to the SFT-only baseline, our model reduces the False Alarm Rate by 47.3% while achieving a competitive F1-score, proving its effectiveness for practical, real-world air quality forecasting systems on long lead time scenarios.

1. Introduction

Atmospheric particulate matter, such as $PM_{2.5}$ and PM_{10} , poses serious public health risks by aggravating respiratory and cardiovascular diseases, and disrupting urban transportation, industrial operations, and power demand. Accurate long lead time forecasts of PM concentrations (48–120 hours) are essential for issuing public alerts, enforce-

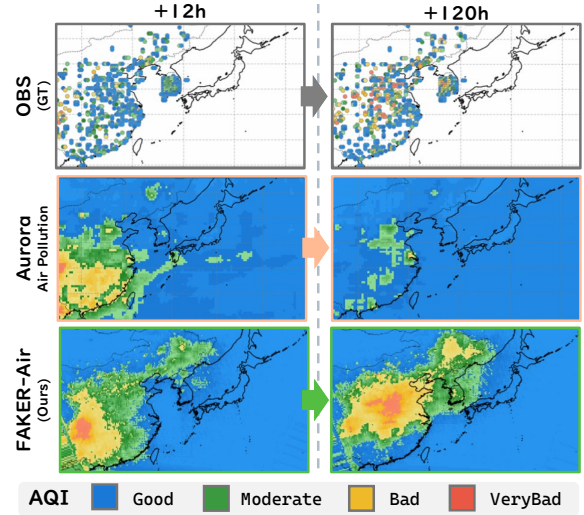


Figure 1. **Illustration of $PM_{2.5}$ predictions.** Our method effectively captures the dynamic temporal variations in PM concentration over time, whereas Aurora [6] fails to reflect such changes.

ing emission controls, and protecting vulnerable populations [1, 23, 27, 35, 40]. However, forecast accuracy deteriorates rapidly beyond short horizons due to complex spatio-temporal interactions among meteorology, emissions, and terrain [46]. This degradation is particularly severe in East Asia, where global models increasingly fail to detect severe pollutions [42, 43, 45], as in Figure 1. Our objective is to achieve stable long horizon PM forecasting with reliable air quality classification suitable for real-time operational warning systems at the target region.

Recent advances in deep learning have produced data-driven weather and air quality models that rival numerical weather prediction (NWP) systems in accuracy and efficiency [10, 18, 39]. Foundation models such as Aurora, GraphCast, and Pangu-Weather learn global atmospheric dynamics from large-scale reanalyses including ERA5, GFS, and CAMS [5, 6, 12, 15, 21, 29]. Notably, Aurora is the only open-source PM forecasting model, making it our baseline. At the regional scale, hybrid convolutional-

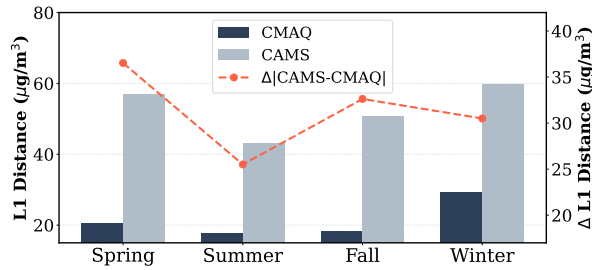


Figure 2. **The seasonal L1 distance error compared with OBS (↓ is better).** Unlike global datasets (CAMS), our locally developed datasets (CMAQ) show low error with real observation.

transformer architectures capture spatio-temporal pollutant transport for PM forecasting [13, 47].

However, when evaluated against ground-based observations (OBS) in East Asia, reanalysis products exhibit large systematic biases and limited operational usability. For instance, CAMS [12], a key training source for foundation models, deviates from ground observations by an average of $52.66 \mu\text{g}/\text{m}^3$ in China and Korea, and suffers from update latencies of a few days. Such limitations, (1) low regional accuracy and (2) lack of real-time availability, stem from data imbalance and physical divergence: East Asia comprises less than 15% of global training coverage, yet contributes over 60% of severe PM exposure. This clearly causes global models to underfit local dynamics.

To address both issues, we release a regional dataset spanning 2016–2023 (8+ years) that pairs real-world **OBS** from 532 Korean and 1,290–1,781 Chinese stations and high resolution Community Multiscale Air Quality (**CMAQ**) reanalysis at 27 km resolution for Korea and China. Our OBS data provides ground-truth measurements at 6 hour intervals, enabling accurate model supervision. CMAQ, tailored for East Asian meteorology and emissions, reduces error to $21.33 \mu\text{g}/\text{m}^3$, a 59.5% improvement over CAMS. Critically, CMAQ-driven forecasts can be initialized within hours from local observations, eliminating the 5 day update delay of global datasets such as CAMS. Training on this unified CMAQ–OBS dataset yields region-aware and operationally real-time ready models.

Once our regional CMAQ–OBS dataset ensures regional accuracy and real-time availability, we establish a strong baseline by supervised training an Aurora-based 3D encoder-decoder on localized data. Although this baseline captures East Asian aerosol dynamics, it faces two limitations. First, long-range forecasting requires sequential 6-hour rollouts, yet teacher forcing exposes the model only to ground-truth states. This causes early inference errors to propagate across future steps. Second, the squared error objective treats all deviations uniformly and fails to capture the asymmetric costs of air-quality decisions, resulting in frequent false alarms despite high predictive accuracy. To address these limitations, we introduce **FAKER-Air** (Forecast Alignment via Knowledge-guided Expected-Reward), a two stage framework built on three core innovations.

First, we introduce a temporal accumulation loss to enforce temporal consistency during supervised finetuning (SFT). Long horizon forecasting proceeds in sequential 6-hour steps. Each step consumes the previous prediction. Teacher forcing feeds only ground truth during training, so the model never sees its own rollouts, creating a train-test mismatch known as exposure bias [4, 33]. At inference, small early errors propagate across steps. We supervise N-step trajectories with the temporal accumulation loss. The loss penalizes stepwise errors along the rollout and reduces exposure bias by stabilizing long-range forecasts.

Temporal accumulation loss still optimizes squared error and remains agnostic to operational costs. Our confusion analysis of the SFT baseline shows many false alarms in clean air levels and strong detection for severe pollution cases. This pattern reflects the symmetric penalty of regression objectives and the heavy influence of large residuals at peaks, which shifts predictions upward in uncertain cases.

To mitigate overestimate problems, we adopt Group Relative Policy Optimization (GRPO) [38] with a class-wise Air Quality Index (AQI) [20] reward to align decisions with operational costs. The reward assigns stronger penalties to false alarms in Good and Moderate. It assigns higher gains for true positives and stronger penalties for misses in Bad and VeryBad to preserve recall. GRPO updates the policy by ranking multiple rollouts for the same input and by increasing the likelihood of higher reward trajectories.

Finally, we employ curriculum rollout scheduling to stabilize long lead optimization during GRPO training. Direct training with a long horizon increases the variance of return estimates and weakens credit assignment. Later states depend on the model’s own predictions, so early errors move the state distribution off manifold. Training starts with short horizons such as 6 hours and extends to 24 hours as learning progresses. The curriculum reduces gradient variance in early training and yields stable updates at long lead times.

Our novel framework improves operational reliability by introducing policy optimization into spatio-temporal forecasting for the first time. Experiments show that FAKER-Air reduces the FAR by 47.3%, while maintaining strong F1-scores for all AQI classes. These advances validate the system’s value for real-world air quality warnings.

Our work enables reliable localized long horizon PM forecasting with the following key contributions:

- **Regional Dataset for Real-Time Forecasting.** We release the first CMAQ–OBS dataset for East Asia, reducing errors by 59.5% compared to CAMS and supporting real-time initialization from 1,822+ monitoring stations.
- **Two-Stage Training Framework.** We combine SFT with multi-step temporal accumulation loss for temporal consistency and introduce GRPO with curriculum rollout and class-wise rewards for decision-aware optimization.

- **Operational Reliability.** Our model improves F1-score by $3.5\times$ over Aurora and reduces the FAR by 47.3%, achieving balanced performance when evaluate on OBS.

2. Related Work

2.1. Earth system models and datasets

Conventional numerical weather prediction (NWP) and earth system models (ESM) [18] couple atmospheric, oceanic, and land processes through primitive equations, but they remain computationally expensive, sensitive to initial conditions, and often inconsistent across modeling systems [2]. The Coupled Model Intercomparison Project (CMIP) [25] provides a standardized framework to evaluate these discrepancies and has generated large datasets that have enabled recent data-driven approaches.

Deep learning has accelerated progress in this direction. Large-ensemble models [44] have demonstrated sub-seasonal forecasting skill, while generative models for short-term precipitation prediction [34] capture local spatio-temporal variability. Subsequent advances include FourCastNet [30] using Fourier Neural Operators for global forecasts and GraphCast [21] employing graph neural networks for accurate medium-range prediction. Transformer-based models such as ClimaX [28] and Pangu-Weather [5] further unified diverse forecasting tasks, and physics-informed approaches such as ClimODE [41] improved temporal consistency. Aurora [6] extends this trend through large scale pretraining on multimodal geoscientific data. Critically, Aurora is the only open-source foundation model that explicitly includes PM forecasting, making it the sole publicly available baseline for comparative evaluation.

Building on these developments, our work targets regional scale, real-time PM forecasting. Unlike global models, our focus is on capturing fine-grained spatial variability and local temporal dynamics for operational applications.

2.2. Alignment Training

Recent advances in alignment training offer an alternative to purely supervised objectives by optimizing task- or preference-aware rewards. Reinforcement learning from human feedback (RLHF) [9] formalizes this using the Bradley-Terry (BT) model [7] to represent pairwise preferences, with policy optimization methods such as PPO maximizing expected reward under a KL constraint. However, online RL remains unstable and computationally expensive, motivating direct alignment methods.

Direct Preference Optimization (DPO) [31] removes the need for an explicit reward model by deriving a closed-form likelihood objective from the BT model, effectively treating preference learning as a classification task. Recent work links DPO to an MDP interpretation in which the model implicitly defines a policy π_θ , and the objective approxi-

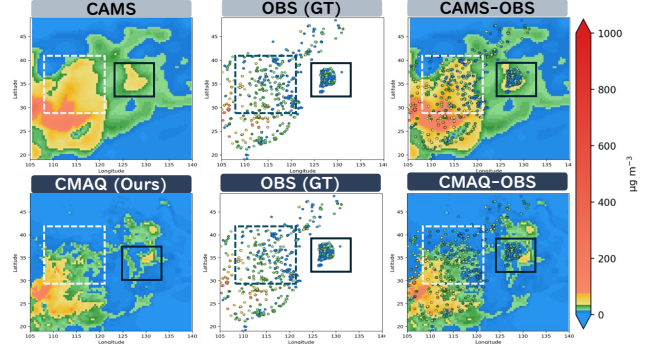


Figure 3. **Comparison of CAMS and CMAQ (ours) with OBS.** CMAQ achieves lower regional error and near real-time availability, enabling stable long horizon forecasting.

mates optimizing $Q(s, a)$ toward the optimal $Q^*(s, a)$ under Bellman consistency [3, 32]. This perspective connects reinforcement-style value learning with SFT.

Several Direct Alignment Algorithms (DAA) build on this idea. ORPO [17] aligns policies via preference-weighted likelihood without a reference model, and SimPO [26] simplifies alignment through implicit reward estimation. Group-Relative Policy Optimization (GRPO) [38], used in our framework, replaces absolute rewards with relative rankings of multiple rollouts from the same context, improving stability without critics or expensive reward modeling. In our setting, GRPO aligns predictions with operational goals such as reducing false alarms and improving detection of severe pollution, bridging supervised learning and decision-centered policy optimization.

3. Dataset

We construct and release the **CMAQ-OBS Regional Air Quality Dataset**, which jointly achieves (1) observation-validated regional accuracy and (2) real-time operational readiness. Existing global reanalysis datasets lack the capacity to satisfy both requirements simultaneously. Global datasets such as CAMS suffer from large regional biases due to coarse emissions and chemistry representations, and their multi-day update latencies prevent timely alert issuance. By integrating sparse ground-observation values with dense physics-driven regional CMAQ reanalysis across China and Korea, our dataset overcomes both limitations, establishing the foundation for reliable long horizon air quality forecasting in East Asia. Details on each dataset are in the supplementary materials.

Station-based Observations (OBS). OBS dataset comprises 6 hour ground-level measurements of $\text{PM}_{2.5}$, PM_{10} , and O_3 concentrations. As shown in Figure 3, the data is sourced from 532 stations in Korea through the AirKorea network and 1,290–1,781 stations in China via the Airquality monitoring system, spanning the period from January

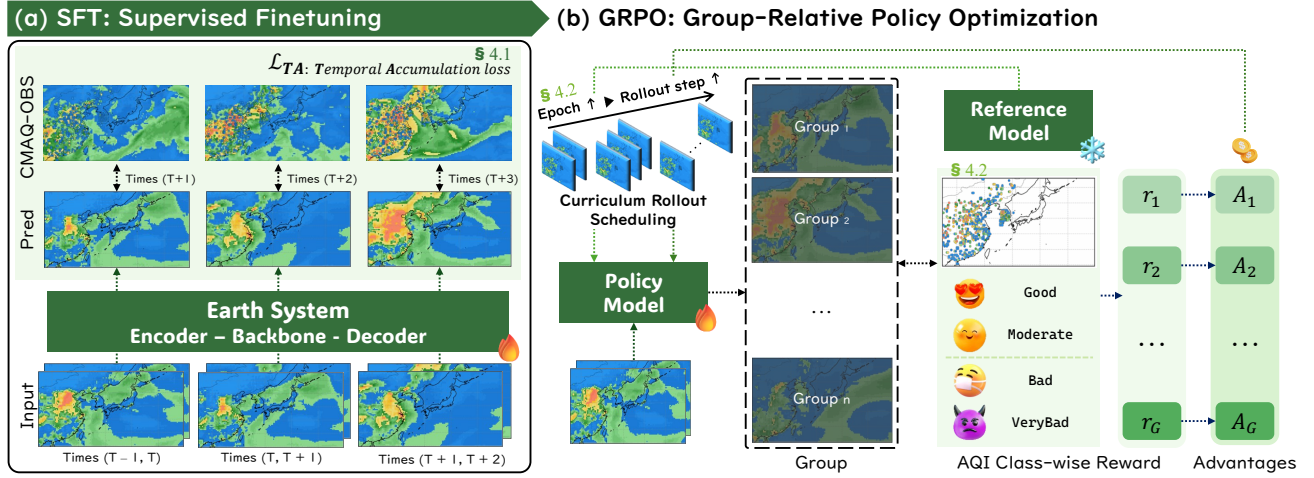


Figure 4. **Overall pipeline of FAKER-Air.** Our two-stage training framework begins with supervised fine-tuning (SFT) with rollout loss, followed by Group-Relative Policy Optimization (GRPO). During GRPO, multiple trajectory groups are evaluated using AQI-based rewards to guide policy updates, with the rollout horizon gradually increasing to enable long-term predictions.

2016 to June 2024. The station-based point observations are collected at 6-hour temporal resolution. For our modeling framework, we spatially interpolate these observations onto the CMAQ grid at 27 km resolution, producing structured fields aligned with our modeling domain. Each gridded OBS field provides surface-level pollutant concentrations. These fields serve as both input features and ground truth targets, split into training and test sets. Critically, they capture real-time atmospheric conditions without the multi-day update delays inherent in global reanalysis products. The Korean observations are complemented by meteorological measurements from 94 ASOS sites and 349 AWS stations and Chinese meteorological observations from Wyoming.

CMAQ. Community Multiscale Air Quality (CMAQ) produces a spatially continuous field spanning 2016–2023 that covers the entire model domain, generating predictions for every grid cell at each time step and providing complete regional coverage beyond individual station locations, as shown in Figure 3. Unlike point-based OBS, CMAQ delivers domain-wide gridded fields that fill spatial gaps with physics-consistent aerosol dynamics, enabling the model to learn transport, boundary conditions, and dispersion patterns. When validated against ground truth, CMAQ tailored to East Asian meteorology and emissions achieves an average error of $21.33 \mu\text{g}/\text{m}^3$, representing a 59.5% improvement over CAMS ($52.66 \mu\text{g}/\text{m}^3$). It also supports initialization within hours from locally available observations, satisfying real-time operational requirements. Besides, its multivariate spatial continuity provides physically grounded priors that mitigate distribution shift during auto-regressive rollouts and prevent the long horizon degradation common in teacher-forced training. By supplying coherent structural signals across seasons and regions, CMAQ enhances generalization under the sparse and variable pollution patterns of East Asia.

4. Method

This section introduces our two stage training framework, **FAKER-Air** (Forecast Alignment via Knowledge-guided Expected-reward Reinforcement learning), for long horizon air quality forecasting. As illustrated in Figure 4, we first describe Stage 1, which establishes fundamental predictive capacity via SFT with temporal accumulation loss, then present Stage 2, which further improves operationally reliable forecasting by directly optimizing decision-centered rewards. This second stage complements SFT by addressing its remaining limitations related to over-prediction bias and asymmetric operational costs.

4.1. Stage 1: SFT with temporal accumulation loss

We begin with SFT to train a base model capable of learning regional aerosol dynamics from historical CMAQ and OBS data. As illustrated in Figure 4(a), given a sequence of input grids $\mathbf{x}_{1:T}$ and the next-step target \mathbf{y}_{T+1} , the model f_θ learns to minimize the Mean Squared Error (MSE) loss:

$$\mathcal{L}_{\text{SFT}} = \mathbb{E}_{\mathbf{x}, \mathbf{y}} [\|f_\theta(\mathbf{x}_{1:T}) - \mathbf{y}_{T+1}\|_2^2]. \quad (1)$$

This supervised stage captures the coarse-scale spatio-temporal structure of pollutant transport and builds a strong baseline for downstream optimization. It allows the model to produce physically consistent concentration fields over multi hour horizons by leveraging the spatial encoder-decoder backbone. Although SFT provides a straightforward way to adapt the pretrained Aurora-like model to a regional domain, we observe a critical limitation when applying it to long horizon PM forecasting.

Addressing error accumulation with Temporal Accumulation (TA) loss. Teacher-forced supervised training treats each lead independently and does not expose the model to its own rollout errors, which creates a train-test

mismatch known as exposure bias [4]. This causes small early errors to compound over the horizon and degrade multi-step forecasts [33, 36, 37, 48].

To address exposure bias, we adopt temporal accumulation loss that supervises auto-regressive forecast trajectories over H lead times rather than single-step predictions. At each step $i \in \{1, \dots, H\}$, the model generates predictions \hat{y}_{T+i} conditioned on its own previous outputs in an auto-regressive manner:

$$\hat{y}_{T+i} = f_\theta(\mathbf{x}_{1:T}, \hat{y}_{T+1:T+i-1}), \quad i = 1, \dots, H. \quad (2)$$

The step-wise loss $\ell_i(\theta)$ at each lead time i is computed as a weighted MSE across multiple variable groups. To progressively emphasize longer forecast horizons, we employ linearly increasing step weights $w_i = b + (1 - b) \frac{i-1}{H-1}$ for $H > 1$, where $b \in (0, 1]$. The final temporal accumulation loss aggregates normalized step losses:

$$\mathcal{L}_{\text{TA}}(\theta) = \sum_{i=1}^H \tilde{w}_i \cdot \ell_i(\theta), \quad \text{where} \quad \tilde{w}_i = \frac{w_i}{\sum_{j=1}^H w_j}. \quad (3)$$

By exposing the model to multi-step error accumulation during training, the temporal accumulation loss reduces the distribution shift between teacher-forced training and auto-regressive inference, thereby improving temporal consistency over extended forecast horizons.

4.2. Stage 2: Group-Relative Policy Optimization

Motivation: Decision-cost mismatch. While temporal accumulation improves long horizon stability, the MSE objective remains misaligned with operational decisions. Quadratic loss over-weights large residuals, biases predictions upward in uncertain regimes [19], and can over-smooth spatial structure [22]. Critically, squared error is cost-symmetric, whereas air quality operations are not: missing a severe event (Bad or VeryBad) is more costly than issuing a false alarm under clear air (Good or Moderate) [11]. We therefore add a second stage that directly optimizes a verifiable, cost-sensitive reward that encodes asymmetric penalties for false alarms and misses, aligning policy updates with real-world alerting priorities.

Policy optimization formulation. We cast forecasting as a policy optimization problem. The model f_θ defines a stochastic policy $\pi_\theta(a_t | s_t)$, where the state s_t encodes the spatiotemporal inputs and the action a_t denotes the predicted concentration field at time $t+1$. The optimization objective is to maximize the expected task reward:

$$\mathcal{J}(\theta) = \mathbb{E}_{\pi_\theta} \left[\sum_{t=1}^T r(s_t, a_t) \right], \quad (4)$$

where $r(s_t, a_t)$ is a verifiable AQI-based reward. This reward is used only to evaluate forecast quality. In GRPO,

it is converted into a relative advantage signal rather than being applied directly to the policy gradient.

GRPO mechanism. GRPO [38] extends policy gradient methods by replacing absolute returns with group-wise relative comparisons. Starting from the SFT-trained policy, we generate G trajectories by sampling actions from a Gaussian policy $a = \mu + \sigma\epsilon$, $\epsilon \sim \mathcal{N}(0, I)$, using antithetic pairs for variance reduction. Each trajectory produces a reward $r_t^{(g)}$, forming a group $\mathcal{G}_t = \{(a_t^{(g)}, r_t^{(g)})\}_{g=1}^G$.

Rather than using raw rewards, GRPO converts them into softmax-normalized weights:

$$A_g = \frac{\exp(r_t^{(g)}/\tau)}{\sum_{j=1}^G \exp(r_t^{(j)}/\tau)}, \quad (5)$$

where A_g functions as a relative advantage indicating the performance of action $a_t^{(g)}$ compared with other rollouts under the same state. The policy is updated by weighting log-likelihoods with these advantage-like coefficients:

$$\mathcal{L}_{\text{GRPO}} = -\mathbb{E}_{(a_t^{(g)}, r_t^{(g)}) \in \mathcal{G}_t} \left[A_g \log \pi_\theta(a_t^{(g)} | s_t) \right]. \quad (6)$$

This ranking-based formulation increases the likelihood of actions with higher relative advantage while suppressing unreliable ones, effectively steering the policy toward trajectories that outperform their group peers. As illustrated in Figure 4(b), GRPO evaluates multiple action rollouts for each state, converts their AQI rewards into relative advantages through groupwise normalization, and adjusts the policy accordingly. This process steers the policy toward operationally reliable predictions, reducing false alarms in clean air conditions while preserving high recall for severe pollution events.

Class-wise reward design. To encode asymmetric operational costs, we adopt a class-wise reward function $R(a_t, y_t)$ defined over discrete AQI categories $\mathcal{C} = \{\text{Good}, \text{Moderate}, \text{Bad}, \text{VeryBad}\}$. Let $\hat{c}_t = \text{AQI}(a_t)$ and $c_t = \text{AQI}(y_t)$ denote the predicted and true AQI classes, respectively. The reward follows the binary scheme used in RLVR (Reinforcement Learning with Verifiable Rewards) [38], which provides a verifiable and stable signal for policy comparison:

$$R(a_t, y_t) = \begin{cases} 1, & \text{if } \hat{c}_t = c_t, \\ 0, & \text{otherwise.} \end{cases} \quad (7)$$

This straightforward binary structure allows GRPO to rank trajectories based on verifiable correctness rather than continuous value estimation, simplifying optimization while maintaining stability. Within the group-relative framework,

Table 1. **Ablation Study on SFT for PM_{2.5} and PM₁₀ on long lead time PM forecasting (12-hour intervals up to 120h).** Integrating OBS with CMAQ and extending temporal accumulation loss (\mathcal{L}_{TA}) to T=4 consistently improves F1-scores across all horizons.

PM _{2.5}														
OBS	CMAQ	\mathcal{L}_{TA} (T=2)	\mathcal{L}_{TA} (T=4)	Overall	+12h	+24h	+36h	+48h	+60h	+72h	+84h	+96h	+108h	+120h
Aurora Air Pollution [6]				16.06	48.82	40.07	17.75	15.00	4.04	4.01	1.16	1.72	0.46	1.05
✓	✗	✗	✗	50.74	61.53	53.83	51.57	49.87	48.79	48.47	48.15	47.76	47.68	47.65
✓	✓	✗	✗	54.40	62.56	58.89	56.73	54.42	52.26	51.86	51.36	51.36	51.41	51.38
✓	✓	✓	✗	57.65	65.89	61.99	60.52	57.58	55.48	54.75	54.04	53.76	53.44	53.34
✓	✓	✗	✓	59.90	67.53	64.48	61.83	60.39	59.05	58.23	57.44	56.94	56.54	56.21
				(+9.16)	(+6.00)	(+10.65)	(+10.26)	(+10.52)	(+10.26)	(+9.76)	(+9.29)	(+9.18)	(+8.86)	(+8.56)
PM ₁₀														
OBS	CMAQ	\mathcal{L}_{TA} (T=2)	\mathcal{L}_{TA} (T=4)	Overall	+12h	+24h	+36h	+48h	+60h	+72h	+84h	+96h	+108h	+120h
Aurora Air Pollution [6]				4.73	23.34	14.08	3.38	1.78	0.22	0.23	0.02	0.04	0	0
✓	✗	✗	✗	41.63	61.12	50.80	43.08	39.65	37.11	35.99	35.16	34.80	34.37	34.12
✓	✓	✗	✗	52.65	67.71	62.97	59.30	57.32	55.77	55.09	54.58	54.23	53.84	53.60
✓	✓	✓	✗	54.60	66.68	62.17	57.92	55.16	52.79	50.94	49.86	48.87	48.13	47.36
✓	✓	✗	✓	57.32	66.65	63.01	59.96	57.97	56.07	54.91	53.96	53.39	52.97	52.46
				(+15.69)	(+5.53)	(+12.21)	(+16.88)	(+18.32)	(+18.96)	(+18.92)	(+18.80)	(+18.59)	(+18.60)	(+18.34)

it naturally captures asymmetric operational priorities by rewarding accurate classification in severe pollution cases while discouraging false alarms under clean air conditions. This alignment steers policy updates toward real-world decision objectives in air-quality alerting systems.

Curriculum Rollout (CR) scheduling. To stabilize long horizon learning during GRPO, we introduce Curriculum Rollout (CR) scheduling where the rollout horizon H gradually increases with training epochs. At early epochs, we restrict H to short lead times (e.g., 1-step) and progressively extend to longer horizons (up to 4-steps). Formally:

$$H_e = \min(H_{\max}, \lfloor H_{\min} + \kappa e \rfloor), \quad (8)$$

where e denotes the current epoch and κ controls expansion rate. As illustrated in Figure 4(b), this progressive extension allows the model to master short-term dynamics before tackling uncertain long range forecasts, significantly reducing gradient noise in early training and improving long horizon prediction reliability. By evaluating forecast trajectories over multiple lead times, GRPO implicitly encourages temporal consistency. Unlike SFT, which optimizes per-step snapshots, policy gradients of GRPO are informed by entire forecast sequences spanning long hours. This allows the model to capture long-term dependencies in aerosol transport and accumulation dynamics.

Integration of SFT and GRPO. To the best of our knowledge, the GRPO stage represents the first application of policy optimization to spatio-temporal forecasting, complementing SFT by bridging the gap between numerical accuracy and decision reliability. While SFT establishes a strong baseline and captures the underlying spatio-temporal dynamics, GRPO refines the model through reward-driven

optimization aligned with operational objectives. Its group-relative weighting and class-wise AQI rewards directly address the decision-cost mismatch left by MSE, while curriculum rollout scheduling stabilizes policy learning over extended horizons. Through this two-stage training, the model achieves decision-grade stability in multi-day PM forecasts, reducing the FAR from while maintaining comparable performance as described in Section 5.

5. Experiment

5.1. Metric

We evaluate our framework using both binary and multi-class classification metrics to assess operational reliability and decision-grade forecasting performance. For binary evaluation, the *F1-Score* [14] summarizes event detection performance by jointly considering precision and recall. *FAR* (False Alarm Rate) [16] quantifies the fraction of false alerts among all non-event cases and serves as a key operational metric, since excessive false alarms reduce the practical usability of an alert system. We further report the *CSI* (Critical Success Index) [24], which penalizes both missed events and false alarms and is widely used for assessing rare event forecasting. *Bias* [8] measures systematic over-prediction or under-prediction, with values near 1.0 indicating well-calibrated event frequency. For multi-class AQI evaluation across four pollution levels, we report *F1-Macro*, which treats all pollution classes equally regardless of their frequency, thereby highlighting model performance on rare severe pollution events. *F1-Weighted* accounts for class imbalance by weighting F1-score of classes proportionally to its sample size, providing a more representative overall performance measure. *F1-Micro* aggregates predictions across all classes before computing the score, effectively measuring overall classification accuracy in the multi-class setting.

Table 2. **Ablation on GRPO reward design and curriculum rollout (CR, e=4) for PM_{2.5} over 120h.** For Binary(2-class): Acc, F1, Prec (↑) and FAR (↓); Bias ≈ 1 preferred. For AQI(4-class): Acc, F1-macro, F1-weighted, F1-micro (↑), plus per-class F1.

Config			Binary Metrics					AQI (4-class) Metrics							
Model	Reward	CR	Acc	F1	Prec	FAR	Bias	Acc	F1-macro	F1-weighted	F1-micro	Good	Mod.	Bad	V.Bad
Aurora	–	–	68.93	16.06	68.40	2.24	0.13	34.03	23.43	28.91	34.03	42.49	36.82	11.46	2.96
FAKER-Air _{SFT}	–	–	69.62	59.90	49.69	32.86	1.52	<u>44.03</u>	<u>41.59</u>	<u>43.63</u>	<u>44.03</u>	38.46	47.79	44.92	35.18
FAKER-Air _{GRPO}	MSE	✗	74.50	48.44	<u>61.90</u>	10.54	0.64	43.73	37.57	42.36	43.73	50.24	<u>46.09</u>	33.93	20.04
FAKER-Air _{GRPO}	AQI	✗	71.40	56.28	52.12	24.19	1.17	42.26	40.75	41.94	42.26	49.19	40.05	39.42	<u>34.35</u>
FAKER-Air _{GRPO}	AQI	✓	74.51	<u>56.72</u>	57.98	<u>17.32</u>	0.96	45.16	41.90	44.66	45.16	50.92	44.90	<u>41.80</u>	29.98

5.2. Implementation Details

We conduct a two-stage training procedure on East Asian air quality integrating real-time OBS and CMAQ reanalysis data to enable real-time long horizon localized forecasting. We employ SFT on an Aurora-based 3D encoder-decoder trained with batch size of 8 for 30 epochs with one-cycle LR. We apply rollout loss with a 4 step auto-regressive prediction. GRPO stage trained with batch size 1 for 4 epochs, generating 4 trajectory samples per input using antithetic sampling with common noise and optimizing a class-wise reward function based on discrete AQI thresholds. We use 2016 to 2021 as training, 2022 as validation, and 2023 as test datasets with 2 H200 GPUs distributed data parallel training with random seed 42. Further details are described in the supplementary materials.

5.3. SFT Experimental Results

Table 1 summarizes the effect of SFT components on long horizon forecasting. Training with OBS alone substantially improves F1-scores over Aurora across all horizons (PM_{2.5}: 16.06 → 50.74; PM₁₀: 4.73 → 41.63). Integrating CMAQ reanalysis further enhances overall performance and markedly improves stability for long lead time, indicating that physics-driven continuous fields compensate for regional biases in sparse observations and reduce distribution variability during auto-regressive rollouts, providing more stable conditions to address exposure bias.

Introducing the multi-step rollout loss \mathcal{L}_{TA} provides consistent gains across all horizons. For PM_{2.5}, $\mathcal{L}_{TA}(T = 2)$ raises overall F1 from 54.40 to 57.65, while extending to $T = 4$ yields 59.90, with sustained improvements at extended leads. PM₁₀ exhibits a similar pattern (52.65 → 57.32). By exposing the model to its own predictions during training, these results demonstrate direct mitigation of exposure bias and enhanced temporal consistency, especially beyond 60h where single-step teacher forcing typically suffers from error accumulation.

Overall, SFT with CMAQ-OBS data fusion and rollout-based objectives establishes a robust baseline by addressing exposure bias. Our SFT model achieves about 3.7× improvement in F1 for PM_{2.5} and 12× for PM₁₀ relative

Table 3. **Comparison of Overall Performance.** CSI and FAR Comparison over 120 hours for PM_{2.5} and PM₁₀

PM _{2.5}						
Model	CSI Score (AQI: 4 classes)				FAR↓ (binary)	Macro CSI
	Good	Mod.	Bad	V.Bad		
Aurora	<u>26.98</u>	22.56	6.08	1.50	2.24	14.28
FAKER-Air _{SFT}	23.81	31.40	28.97	21.34	32.86	<u>26.38</u>
FAKER-Air _{GRPO}	34.16	<u>28.95</u>	<u>26.42</u>	<u>17.63</u>	<u>17.32</u>	26.79
	(+7.18)	(+6.39)	(+20.34)	(+16.13)	(−15.54)	(+12.51)
PM ₁₀						
Model	CSI Score (AQI: 4 classes)				FAR↓ (binary)	Macro CSI
	Good	Mod.	Bad	V.Bad		
Aurora	<u>28.84</u>	18.78	1.63	0.38	0.33	12.41
FAKER-Air _{SFT}	28.63	42.43	26.21	18.83	18.44	29.02
FAKER-Air _{GRPO}	36.39	<u>37.53</u>	<u>23.03</u>	<u>15.35</u>	<u>10.81</u>	<u>28.07</u>
	(+7.55)	(+18.75)	(+21.40)	(+14.97)	(−7.63)	(+15.66)

to Aurora, effectively mitigating performance collapse beyond 60–120h. This provides the essential precondition for subsequent policy optimization (Section 4.2) to refine operational cost metrics such as FAR and class-wise metrics.

5.4. GRPO Experimental Results

Table 3 summarizes the impact of GRPO on long horizon AQI classification. While SFT establishes a strong baseline, it suffers from a decision cost mismatch because MSE treats all errors symmetrically. However, operational costs are asymmetric between false alarms and missed severe events. This causes SFT to exaggerate the probability of pollution, yielding a higher FAR despite an improved CSI. GRPO directly addresses this by optimizing class-wise AQI rewards, substantially lowering FAR by 47.3% (32.86 → 17.32) while maintaining stable Macro CSI and achieving near-ideal Bias (1.52 → 0.96), demonstrating that asymmetric rewards resolve the decision cost mismatch left unaddressed by regression-based SFT.

A consistent pattern emerges for PM₁₀, where GRPO cuts FAR by approximately 41% (18.44 → 10.81) while maintaining comparable Macro CSI. The Good category improves substantially, while other classes change modestly, yielding a more conservative and trustworthy operating point for long horizon alerts. These class-wise adjust-

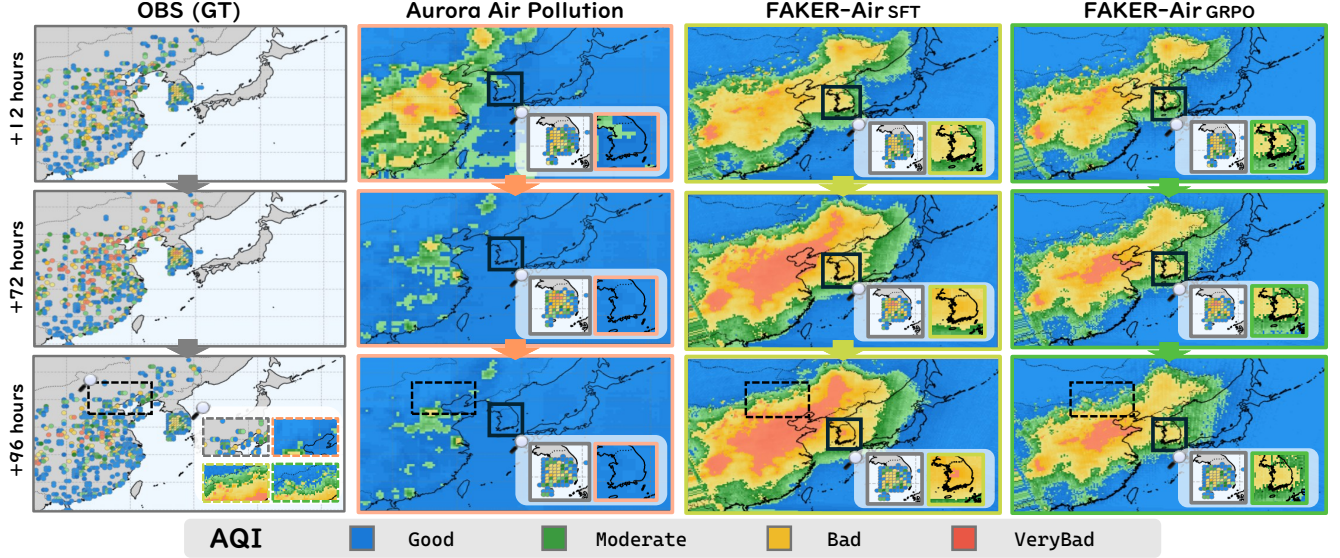


Figure 5. **Qualitative comparison of long horizon $\text{PM}_{2.5}$ forecasts over East Asia.** Aurora rapidly loses regional structure. SFT restores coherent transport but slightly overextends moderate pollution. GRPO prunes these artifacts while preserving high-pollution cores.

ments demonstrate that AQI-based reward of GRPO effectively reduces FAR while preserving overall metrics.

Table 2 provides deeper analysis of how reward design and curriculum rollout drive gains of GRPO. The choice of reward function proves critical: MSE-based reward proves ineffective for policy optimization. In contrast, class-wise AQI rewards achieve balanced performance by penalizing false positives in clean air states, though at the cost of elevated FAR. Introducing curriculum rollout restores reliability, reducing FAR to 17.32 while maintaining F1-score and achieving near-ideal Bias. These results demonstrate that GRPO benefits from both decision-aware rewards and progressively extended rollouts for long horizon stability.

Overall, SFT and GRPO form a complementary pipeline where SFT provides temporal consistency, while GRPO aligns decisions with operational costs via group-relative ranking, class-wise rewards, and rollout scheduling. To the best of our knowledge, this work represents the first application of policy optimization to time-series forecasting on climate, enabled by our CMAQ-OBS dataset that addresses the absence of validated regional baselines and real-time OBS data for East Asia. Our approach produces fewer unnecessary alerts. By leveraging asymmetric rewards and relative ranking, GRPO delivers decision-grade predictions suitable for operational air quality applications.

5.5. Qualitative Results

Figure 5 contrasts spatial predictions at +12h, +72h, and +96h lead times. Aurora rapidly loses mesoscale structure, producing diffuse fields that fail to track the temporal evolution visible in ground-truth observations. In contrast,

FAKER-Air SFT restores coherent spatial patterns and maintains sharp inter-basin contrasts across extended horizons, demonstrating that our temporal accumulation loss effectively suppresses cumulative error propagation during autoregressive rollout. FAKER-Air GRPO further refines these predictions through decision-aware alignment, removing spurious Bad level artifacts that appear in SFT under clean air regimes while retaining high-concentration cores, directly mirroring the quantitative FAR reductions. Notably, at +96h our framework successfully captures transboundary pollution transport, a challenging pattern that Aurora completely fails to resolve. At this extended lead time, where Aurora collapses toward uniform backgrounds, our framework maintains both spatial fidelity and operational reliability across long horizon forecasts.

6. Conclusion

This work addresses the latency and regional limitations of global foundation models for long horizon air quality forecasting in East Asia. We construct and release the CMAQ-OBS dataset that enables real-time initialization for East Asia, providing the research community with validated regional data to advance operational air quality forecasting and public health protection. Moreover, we propose a two stage framework, FAKER-Air, combining SFT with temporal accumulation loss and GRPO with class-wise rewards. Experimental results demonstrate $3.5\times$ improvement in F1-score over Aurora and 47.3% reduction in FAR. By unifying physical modeling with decision-aware optimization, our model balances accuracy and reliability for PM warning systems.

References

- [1] Jonathan O Anderson, Josef G Thundiyil, and Andrew Stolbach. Clearing the air: a review of the effects of particulate matter air pollution on human health. *J Med Toxicol*, 8(2): 166–175, 2012. 1
- [2] V Balaji, Fleur Couvreur, Julie Deshayes, Jacques Gautrais, Frédéric Hourdin, and Catherine Rio. Are general circulation models obsolete? *Proceedings of the National Academy of Sciences*, 119(47):e2202075119, 2022. 3
- [3] Richard Bellman. A markovian decision process. *Journal of Mathematics and Mechanics*, 6(5):679–684, 1957. 3
- [4] Samy Bengio, Oriol Vinyals, Navdeep Jaitly, and Noam Shazeer. Scheduled sampling for sequence prediction with recurrent neural networks. In *Proceedings of the 29th International Conference on Neural Information Processing Systems - Volume 1*, page 1171–1179, Cambridge, MA, USA, 2015. MIT Press. 2, 5
- [5] Kaifeng Bi, Lingxi Xie, Hengheng Zhang, Xin Chen, Xiaotao Gu, and Qi Tian. Accurate medium-range global weather forecasting with 3d neural networks. *Nature*, 619(7970): 533–538, 2023. 1, 3
- [6] Cristian Bodnar, Wessel P Bruinsma, Ana Lucic, Megan Stanley, Anna Allen, Johannes Brandstetter, Patrick Garvan, Maik Riechert, Jonathan A Weyn, Haiyu Dong, et al. A foundation model for the earth system. *Nature*, pages 1–8, 2025. 1, 3, 6
- [7] Ralph Allan Bradley and Milton E. Terry. Rank analysis of incomplete block designs: I. the method of paired comparisons. *Biometrika*, 39(3/4):324–345, 1952. 3
- [8] Harold Brooks, Arthur Witt, and Michael Eilts. Verification of public weather forecasts available via the media. *Bulletin of the American Meteorological Society*, 78, 1997. 6
- [9] Paul F Christiano, Jan Leike, Tom Brown, Miljan Martic, Shane Legg, and Dario Amodei. Deep reinforcement learning from human preferences. In *Advances in Neural Information Processing Systems*. Curran Associates, Inc., 2017. 3
- [10] Shengdong Du, Tianrui Li, Yan Yang, and Shi-Jinn Horng. Deep air quality forecasting using hybrid deep learning framework. *IEEE Transactions on Knowledge and Data Engineering*, 33(6):2412–2424, 2019. 1
- [11] Charles Elkan. The foundations of cost-sensitive learning. In *Proceedings of the 17th International Joint Conference on Artificial Intelligence - Volume 2*, page 973–978, San Francisco, CA, USA, 2001. Morgan Kaufmann Publishers Inc. 5
- [12] European Centre for Medium-Range Weather Forecasts (ECMWF). Cams: Global atmospheric composition forecast data documentation, 2024. Accessed: 2025-11-08. 1, 2
- [13] S. Gul, G. M. Khan, and S. Yousaf. Multi-step short-term PM_{2.5} forecasting for enactment of proactive environmental regulation strategies. *Environmental Monitoring and Assessment*, 194(5):386, 2022. PMID: 35445884, PMCID: PMC9022063. 2
- [14] David J. Hand, Peter Christen, and Nishadi Kirielle. F*: An interpretable transformation of the f-measure, 2021. 6
- [15] H. Hersbach, B. Bell, P. Berrisford, G. Biavati, A. Horeanyi, J. Munoz Sabater, J. Nicolas, C. Peubey, R. Radu, I. Rozum, D. Schepers, A. Simmons, C. Soci, D. Dee, and J.-N. Thepaut. ERA5 hourly data on single levels from 1940 to present. <https://cds.climate.copernicus.eu/cdsapp#/protect/protect/leavevmode@ifvmode/kern-.1667em/relax/dataset/reanalysis-era5-single-levels?tab=overview>, 2018. Accessed: 2025-11-08. 1
- [16] Steven A. Hicks, Inga Strümke, Vajira Thambawita, Malek Hammou, Michael A. Riegler, Pål Halvorsen, and Sravanthi Parasa. On evaluation metrics for medical applications of artificial intelligence. *Scientific Reports*, 12(1):5979, 2022. 6
- [17] Jiwoo Hong, Noah Lee, and James Thorne. Orpo: Monolithic preference optimization without reference model. *arXiv preprint arXiv:2403.07691*, 2024. 3
- [18] James W Hurrell, Marika M Holland, Peter R Gent, Steven Ghan, Jennifer E Kay, Paul J Kushner, J-F Lamarque, William G Large, D Lawrence, Keith Lindsay, et al. The community earth system model: a framework for collaborative research. *Bulletin of the American Meteorological Society*, 94(9):1339–1360, 2013. 1, 3
- [19] Aryan Jadon, Avinash Patil, and Shruti Jadon. A comprehensive survey of regression-based loss functions for time series forecasting. In *International Conference on Data Management, Analytics & Innovation*, pages 117–147. Springer, 2024. 5
- [20] Myung-Il Jung, Seok-Woo Son, Hyemi Kim, and Deliang Chen. Tropical modulation of east asia air pollution. *Nature Communications*, 13(1):5580, 2022. 2
- [21] Remi Lam, Alvaro Sanchez-Gonzalez, Matthew Willson, Peter Wirsberger, Meire Fortunato, Ferran Alet, Suman Ravuri, Timo Ewalds, Zach Eaton-Rosen, Weihua Hu, et al. Learning skillful medium-range global weather forecasting. *Science*, 382(6677):1416–1421, 2023. 1, 3
- [22] Christian Ledig, Lucas Theis, Ferenc Huszar, Jose Caballero, Andrew Cunningham, Alejandro Acosta, Andrew Aitken, Alykhan Tejani, Johannes Totz, Zehan Wang, et al. Photo-realistic single image super-resolution using a generative adversarial network. In *Proceedings of the IEEE conference on computer vision and pattern recognition*, pages 4681–4690, 2017. 5
- [23] Wang Sik Lee, Inha Kang, Sung-Jin Yoon, Hyunjung Kim, Yugeong Sim, Youngjun Park, Jinah Park, and Jinyoung Jeong. Three-dimensional label-free visualization of the interactions of pm_{2.5} with macrophages and epithelial cells using optical diffraction tomography. *Journal of Hazardous Materials*, 456:131678, 2023. 1
- [24] Gashirai K Mbizvo and Andrew J Larner. On the dependence of the critical success index (CSI) on prevalence. *Diagnostics (Basel)*, 14(5), 2024. 6
- [25] Gerald A Meehl, George J Boer, Curt Covey, Mojib Latif, and Ronald J Stouffer. The coupled model intercomparison project (cmip). *Bulletin of the American Meteorological Society*, 81(2):313–318, 2000. 3
- [26] Yu Meng, Mengzhou Xia, and Danqi Chen. Simpo: Simple preference optimization with a reference-free reward.

- Advances in Neural Information Processing Systems*, 37: 124198–124235, 2025. 3
- [27] Katherine Newell, Christiana Kartsonaki, Kin Bong Hubert Lam, and Om P. Kurmi. Cardiorespiratory health effects of particulate ambient air pollution exposure in low-income and middle-income countries: a systematic review and meta-analysis. *The Lancet Planetary Health*, 1(9):e368–e380, 2017. 1
- [28] Tung Nguyen, Johannes Brandstetter, Ashish Kapoor, Jayesh K Gupta, and Aditya Grover. Climax: A foundation model for weather and climate. *arXiv preprint arXiv:2301.10343*, 2023. 3
- [29] National Oceanic and Atmospheric Administration (NOAA). Noaa global forecast system (gfs), 2024. Accessed: 2025-11-08. 1
- [30] Jaideep Pathak, Shashank Subramanian, Peter Harrington, Sanjeev Raja, Ashesh Chattopadhyay, Morteza Mardani, Thorsten Kurth, David Hall, Zongyi Li, Kamyar Azizzadenesheli, et al. Fourcastnet: A global data-driven high-resolution weather model using adaptive fourier neural operators, arxiv. *arXiv preprint arXiv:2202.11214*, 2022. 3
- [31] Rafael Rafailov, Archit Sharma, Eric Mitchell, Christopher D Manning, Stefano Ermon, and Chelsea Finn. Direct preference optimization: Your language model is secretly a reward model. *Advances in Neural Information Processing Systems*, 36:53728–53741, 2023. 3
- [32] Rafael Rafailov, Joey Hejna, Ryan Park, and Chelsea Finn. From r to q^* : Your language model is secretly a q -function. *arXiv preprint arXiv:2404.12358*, 2024. 3
- [33] Marc’Aurelio Ranzato, Sumit Chopra, Michael Auli, and Wojciech Zaremba. Sequence level training with recurrent neural networks. *arXiv preprint arXiv:1511.06732*, 2015. 2, 5
- [34] Suman Ravuri, Karel Lenc, Matthew Willson, Dmitry Kangin, Remi Lam, Piotr Mirowski, Megan Fitzsimons, Maria Athanassiadou, Sheleem Kashem, Sam Madge, et al. Skilful precipitation nowcasting using deep generative models of radar. *Nature*, 597(7878):672–677, 2021. 3
- [35] Markus Reichstein, Vitus Benson, Jan Blunk, Gustau Camps-Valls, Felix Creutzig, Carina J. Fearnley, Boran Han, Kai Kornhuber, Nasim Rahaman, Bernhard Schölkopf, José María Tárraga, Ricardo Vinuesa, Karen Dall, Joachim Denzler, Dorothea Frank, Giulia Martini, Naomi Nganga, Danielle C. Maddix, and Kommy Weldemariam. Early warning of complex climate risk with integrated artificial intelligence. *Nature Communications*, 16(1):2564, 2025. 1
- [36] Steven J. Rennie, Etienne Marcheret, Youssef Mroueh, Jarret Ross, and Vaibhava Goel. Self-critical sequence training for image captioning. In *Proceedings of the IEEE conference on computer vision and pattern recognition*, 2017. 5
- [37] Florian Schmidt. Generalization in generation: A closer look at exposure bias, 2019. 5
- [38] Zhihong Shao, Peiyi Wang, Qihao Zhu, Runxin Xu, Junxiao Song, Xiao Bi, Haowei Zhang, Mingchuan Zhang, YK Li, Yang Wu, et al. Deepseekmath: Pushing the limits of mathematical reasoning in open language models. *arXiv preprint arXiv:2402.03300*, 2024. 2, 3, 5
- [39] Jimeng Shi, Azam Shirali, Bowen Jin, Sizhe Zhou, Wei Hu, Rahuul Rangaraj, Shaowen Wang, Jiawei Han, Zhao-nan Wang, Upmanu Lall, et al. Deep learning and foundation models for weather prediction: A survey. *arXiv preprint arXiv:2501.06907*, 2025. 1
- [40] Z. Tao, M. Chin, M. Gao, T. Kucsera, D. Kim, H. Bian, J. Kurokawa, Y. Wang, Z. Liu, G. R. Carmichael, Z. Wang, and H. Akimoto. Evaluation of nu-wrf model performance on air quality simulation under various model resolutions – an investigation within the framework of mics-asia phase iii. *Atmospheric Chemistry and Physics*, 20(4):2319–2339, 2020. 1
- [41] Yogesh Verma, Markus Heinonen, and Vikas Garg. Climode: Climate and weather forecasting with physics-informed neural odes. *arXiv preprint arXiv:2404.10024*, 2024. 3
- [42] Zhili Wang, Lei Lin, Yangyang Xu, Huizheng Che, Xiaoye Zhang, Hua Zhang, Wenjie Dong, Chense Wang, Ke Gui, and Bing Xie. Incorrect asian aerosols affecting the attribution and projection of regional climate change in cmip6 models. *npj Climate and Atmospheric Science*, 4(1):2, 2021. 1
- [43] Jing Wei, Zhanqing Li, Alexei Lyapustin, Jun Wang, Oleg Dubovik, Joel Schwartz, Lin Sun, Chi Li, Song Liu, and Tong Zhu. First close insight into global daily gapless 1 km PM(2.5) pollution, variability, and health impact. *Nat Commun*, 14(1):8349, 2023. 1
- [44] Jonathan A Weyn, Dale R Durran, Rich Caruana, and Nathaniel Cresswell-Clay. Sub-seasonal forecasting with a large ensemble of deep-learning weather prediction models. *Journal of Advances in Modeling Earth Systems*, 13(7):e2021MS002502, 2021. 3
- [45] Man Yue, Xinyi Dong, Minghuai Wang, Louisa K. Emmons, Yuan Liang, Dan Tong, Yawen Liu, and Yaman Liu. Modeling the air pollution and aerosol-pbl interactions over china using a variable-resolution global model. *Journal of Geophysical Research: Atmospheres*, 128(22):e2023JD039130, 2023. e2023JD039130 2023JD039130. 1
- [46] Nur’atiah Zaini, Lee Woen Ean, Ali Najah Ahmed, Marlinda Abdul Malek, and Ming Fai Chow. Pm2.5 forecasting for an urban area based on deep learning and decomposition method. *Scientific Reports*, 12(1):17565, 2022. 1
- [47] K. Zhang, X. Yang, H. Cao, J. Thé, Z. Tan, and H. Yu. Multi-step forecast of PM2.5 and PM10 concentrations using convolutional neural network integrated with spatial-temporal attention and residual learning. *Environmental International*, 171:107691, 2023. Epub 2022 Dec 10, PMID: 36516675. 2
- [48] Deyu Zhou, Quan Sun, Yuang Peng, Kun Yan, Runpei Dong, Duomin Wang, Zheng Ge, Nan Duan, and Xiangyu Zhang. Taming teacher forcing for masked autoregressive video generation. In *Proceedings of the IEEE conference on computer vision and pattern recognition*, pages 7374–7384, 2025. 5